THE JOURNAL OF PHYSICAL CHEMISTRY Letters

Letter

pubs.acs.org/JPCL

Thermodynamic Analysis of Multiply Twinned Particles: Surface Stress Effects

Srikanth Patala,[†,⊥] Laurence D. Marks,[†] and Monica Olvera de la Cruz*[,†,‡]

[†]Department of Materials Science and Engineering, Northwestern University, Evanston, Illinois 60208, United States

[‡]Department of Chemistry, Northwestern University, Evanston, Illinois 60208, United States

Supporting Information

ABSTRACT: In nanoparticle technologies, such as SERS, fuel cell catalysis and data storage, icosahedral and decahedral nanoparticles, owing to their defect structure, provide higher functionality than their single-crystal Wulff counterparts. However, precise control on the yield of multiply twinned structures during solution synthesis has been challenging. In particular, it is difficult to synthesize icosahedral structures due to the high volumetric strain energy associated with the disclination defects and the transition to decahedral morphologies. In this Letter, we elucidate the role of surface stresses in influencing the thermodynamic stability of multiply twinned particles. Increasing the surface stresses inhibits the formation of decahedral structures and increases the likelihood of synthesizing metastable icosahedral particles. Analogously, large decahedral particles may be stabilized by decreasing the surface stresses. Therefore, by tailoring the solution chemistry to influence the surface stresses, greater control over the synthesis of multiply twinned structures can be achieved.

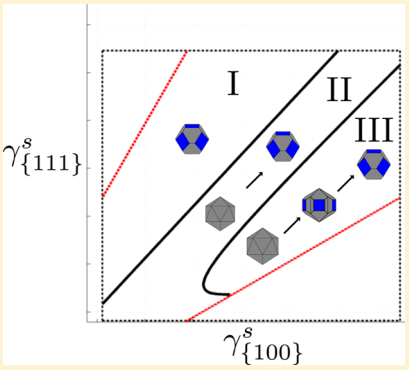

SECTION: Physical Processes in Nanomaterials and Nanostructures

In the synthesis of small metallic nanoparticles, crystallization usually occurs with the formation of icosahedral (Ic) and decahedral (Dh) morphologies, which contain multiple twin boundaries and disclination line defects. The Ic structure consists of 20 tetrahedral subunits with 30 twin boundaries, and Dh particles are formed by joining together five tetrahedral subunits along five twin boundaries. The structure of these small particles, due to their tendency to form such multiply twinned structures with forbidden crystallographic symmetries, has been a topic of interest for over a century.[1,2] These morphologies are also inherently strained and present unique and exciting prospects in metallic nanoparticle technologies.

For instance, gold and silver icosahedra were found to have much higher electrocatalytic activity than their sphere-like analogues.[3,4] The Ic nanoparticles are also of great interest in magnetic applications. Compared to their single crystal morphologies, large magnetic moments were observed in Ic nanoparticles[5] and surprising oxidation resistance has been observed in Ic FePt nanoparticles,[6,7] an important consideration for obtaining high signal-to-noise ratio in magnetoresistive sensors.[8] The Dh-shaped nanoparticles also offer unique opportunities for improved performance in plasmonic,[9,10] optical,[11−13] and catalytic applications.[14]

In order to exploit the unique advantages offered by the distinct structural features of Ic and Dh morphologies, it is essential to obtain precise control during the synthesis of these nanoparticles. From a thermodynamic point of view, it is believed that the Ic nanoparticles are only stable at very small sizes. At intermediate sizes they transition to the Dh morphology and at larger sizes the transition to the single crystal (Sc) Wulff shape occurs. Atomistic simulations of nanoparticle morphologies have verified this trend.[15−19] However, under certain experimental conditions, it is possible to grow large Ic structures by tailoring the solution growth conditions.[20−24] Even when a Dh seed is used, in a slow reaction kinetics regime (at pH 7), asymmetric growth of Ic structures rather than decahedra has been observed.[25] Whereas these inconsistencies have been attributed to kinetic effects, a rigorous investigation of thermodynamic stability, accounting for different experimental conditions, has never been performed.

One of the major obstacles to the thermodynamic analysis of multiply twinned particles (MTPs) is the accurate computation of elastic strain energy arising due to the disclination line defects. Prior theoretical works have addressed the thermodynamic stability aspects for MTPs (see for example Gonzalez et al.[26]), however, we are not aware of calculations that include the strain energy of the disclination defect in an anisotropic elastic medium. In ref 27, we performed finite element analysis to compute the dependence of elastic strain energy of the disclination line defect for Dh shapes with varying geometries. In this Letter, we compute the strain energy of the disclination line defects in the Ic morphology. We incorporate the effect of surface energies and stresses, and present the thermodynamic analysis of the stability regimes for MTPs. We observe that, in the region where MTPs are thermodynamically viable, higher

Received: July 16, 2013
Accepted: August 28, 2013
Published: August 28, 2013

   dx.doi.org/10.1021/jz401496d | J. Phys. Chem. Lett. 2013, 4, 3089−3094

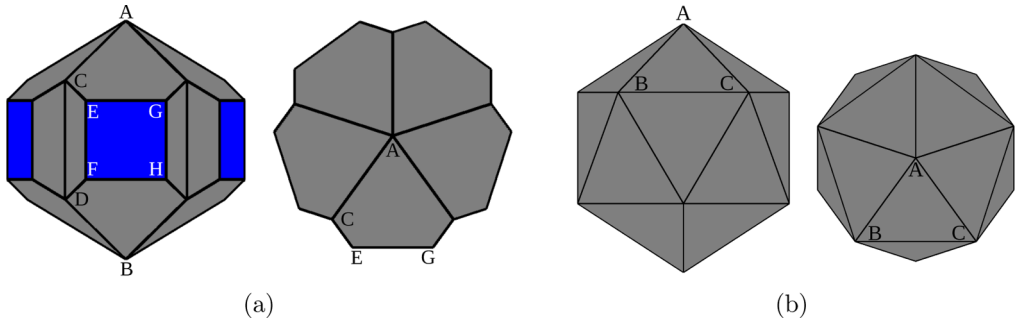

Figure 1. Schematics of typical multiply twinned nanoparticles: (a) The decahedral morphology with re-entrant grooving along the twin boundaries characterized by the grooving-factor $\beta = EG/a = 0.5$ and the aspect ratio $h_r = AB/a = 1.5$, where $a = AC + CE$.[27] The gray and blue colored surfaces are {111} and {100} facets respectively. (b) The icosahedral morphology used in the finite element analysis without re-entrant grooving for simplicity.

surface stresses result in an increase in the likelihood of obtaining Ic nanoparticles and lower surface stresses stabilize the formation of Dh morphologies. This phenomena emphasizes the importance of measuring and controlling surface stresses in the solution synthesis of nanoparticles.

The free energy equation for nanoparticles including the significant energy contributions is:

$$\begin{aligned} G(T) &= G_V(T) + G_S(T) + (\text{higher order terms}) \\ &\approx V(\Delta\bar{G}_f + W_V) + A_{\{111\}}\gamma_{\{111\}} + A_{\{100\}}\gamma_{\{100\}} \\ &\quad + A_t\gamma_t \end{aligned} \tag{1}$$

where the subscripts V and S refer to the volumetric and surface free energy contributions respectively, and the higher order terms comprised of the edge and corner energies are neglected. $\Delta\bar{G}_f$ is the free energy of formation of a crystal without any defects. W_V is the strain energy of the disclination defect per unit volume in the MTPs and is computed using finite element analysis. A and γ refer to the surface area and the surface free energy per unit area of a crystallographic facet respectively. Only {111} and {100} facets are considered, assuming the strong-faceting model for anisotropic surfaces.[28] The subscript t refers to the {111} twin boundary energy, and A_t is greater than zero only for the Dh and Ic structures.

At the nanoscale, surface stresses play an important role in the thermodynamic analysis of the stability of MTPs. The energetic contribution due to the lattice compression is important;[29] however, when transitions among various morphologies of the same metal are considered, the differences in energies due to the lattice compression are negligible and can be ignored. Another significant contribution is the change in the surface free energy (γ) due to the surface strain. Since the surfaces of Ic and Dh nanoparticles are elastically strained, the surface stress term will play an important role in determining the transition sizes among various morphologies. The surface free energies and stresses are environment dependent and will be discussed further in the following paragraphs. The twin boundary energies, which do not depend on the surrounding environment, are estimated using ab initio calculations.[29]

MTPs contain single crystal tetrahedral units which are not space filling in the unstrained state. However, these gaps are filled by strained tetrahedral units, joined together at the {111} twin boundaries, resulting in disclination defects.[30,31] The balance between the strain energy of the disclination defects and the surface energies results in the stability of these MTPs at small sizes. The Ic and Dh morphologies contain 20 and 5 tetrahedral units, respectively; the solid angle deficiency is higher in the Ic particle resulting in larger elastic strain energy in the icosahedron compared to the decahedron. Therefore, Ic particles are only stable at very small sizes. The disclination strain energy is proportional to the volume of the particle, and, as the size increases, MTPs transition into the Sc Wulff shapes. Typical geometries of the Dh and Ic morphologies are shown in Figure 1.

In ref 27, we performed finite element simulations in ABAQUS[32] to compute the strain energy of the disclination defect for Dh structures. To explore the stability of the Ic shapes, we extend the analysis to the icosahedron and compute the strain energy of the disclination defects. We build the icosahedron model with twenty tetrahedral units joined together with wedge gaps, as shown in Figure S1(a) in the Supporting Information (SI), and perform finite element simulations in two steps as described in ref 27. In the first step, we apply displacement boundary conditions to the surfaces of the tetrahedral units such that the wedge gaps are closed and the surfaces overlap (Figure S1(b)). In the second step, we apply the tie constraints to the surfaces (Figure S1(c)); remove the boundary conditions; and equilibrate the icosahedron model.

In Table 1, we compare the strain energies computed using FEA to the best available analytical estimates derived for both the Ic and Dh particles in Howie and Marks[29] (referred to as HM in the rest of the article). HM obtain the analytical estimates using an isotropic approximation for the elastic medium. The estimates of the disclination strain energy per unit volume of the Ic and Dh structures are $W_V^{Dh} = \mu\varepsilon_{Dh}^2/[4(1 -$

Table 1. Comparison of the Strain Energy of the Disclination Defect in Decahedral and Icosahedral Shapes to the Isotropic Elastic Estimate in HM[a]

material	morphology	ABAQUS (10^6 J)	HM isotropic estimate (10^6 J)
gold	decahedral	3.682	5.033
	icosahedral	85.605	58.355
silver	decahedral	3.725	4.997
	icosahedral	78.520	54.641

[a]For decahedral particles, the geometry used is such that $\beta = 0.5$ and $h_r = 1.5$ (refer to Figure 1 for the definition of the parameters β and h_r). The elastic constants used for ABAQUS computations and the isotropic constants used in HM are provided in Table S1 of the Supporting Information.

dx.doi.org/10.1021/jz401496d | J. Phys. Chem. Lett. 2013, 4, 3089−3094

$\nu)]$ and $W_V^{Ic} = (2\mu\varepsilon_{Ic}^2/9)[(1+\nu)/(1-\nu)]$ respectively. ε quantifies the power of the disclination defects with $\varepsilon_{Dh} = [2\pi - 5\arccos(1/3)]/2\pi$ and $\varepsilon_{Ic} = 3\varepsilon_{Dh}$; μ is the shear modulus; and ν is the Poisson's ratio. The strain energy of the decahedron, computed using FEA and anisotropic elastic constants,[33,31] is ~0.75 times the analytical estimate obtained in HM.[27] For the icosahedron, the computed strain energy is ~1.45 times the analytical estimate.

Surface stresses arise when the applied strain modifies the structure of the surface while keeping the number of lattice sites constant (as opposed to creating or destroying the surface without changing its structure). Using the Lagrangian definition for the surface area, surface stress can be formulated as the change in the surface energy as:[29,34]

$$\gamma_{\{hkl\}} = \gamma^s_{\{hkl\}} + \sum_{ij} e_{ij}\frac{\partial\gamma_{\{hkl\}}}{\partial e_{ij}} = \gamma^s_{\{hkl\}} + \sum_{ij} e_{ij}g^{ij}_{\{hkl\}} \quad (2)$$

where $\gamma^s_{\{hkl\}}$ is the free energy of the unstrained surface and e_{ij} denote the components of the in-plane strain tensor. Since different crystallographic facets have distinct atomic structures, they respond differently to the applied strain. Therefore, the response of a surface to strain is also anisotropic and a function of the normal vector to the crystal facet. In general, the surface stress tensor is a 2 × 2 symmetric matrix. However, for crystallographic facets consisting of a 3-fold (or higher) rotational symmetry axis, the surface stress may be denoted by a scalar $g_{\{hkl\}}$ in the coordinate system of the set of the principal axes.[35] Qualitatively, surface stress is a measure of the surface resistance to the in-plane surface strain. $g_{\{hkl\}}$ is positive/negative if the surface is in an extended/compressed state in the bulk as compared to the equilibrium arrangement of the atoms in the two-dimensional surface layer isolated from the bulk.

We further assume that the surface stress is proportional to the unstrained surface free energy, i.e. $g_{\{hkl\}} = g\gamma^s_{\{hkl\}}$, where g is called the "surface stress factor".[29] This assumption allows for the separation of the parameter g that depends only on the solution chemistry and not on the type of the crystallographic facet. As mentioned in the previous paragraph, the sign of g depends on the stress state (tensile or compressive) of the surface. The magnitude of g depends on the extent of the deviation in the atomic structure of the facet in its bulk state as compared to its isolated two-dimensional layer. An approximate estimate of the surface stress factor g for a clean surface of Pt{111} is provided in the Supporting Information.

To compute the change in the surface free energy due to the disclination defect, we assume that the strain on the surface of the MTPs is a constant denoted by $\bar{e}_s$[29] such that $\bar{e}_s^{Dh} = \varepsilon_{Dh}/2$ and $\bar{e}_s^{Ic} = 2\varepsilon_{Ic}/3$ for Dh and Ic morphologies, respectively. These assumptions are compatible with the strain solutions derived in HM.[29] Therefore, the change in the surface free energy due to surface strain in multiply twinned nanoparticles can be expressed as

$$\gamma_{\{hkl\}} = \gamma^s_{\{hkl\}}(1 + g\bar{e}_s) \quad (3)$$

where g and $\gamma^s_{\{hkl\}}$ depend on the environment in which the particles are grown and $\bar{e}_s$ depends on the morphology (Ic, Dh, or Sc) of the particle. Since the surface free energies and the stresses are difficult to determine a priori, we vary these quantities in the thermodynamic analysis. For example, $\gamma^s_{\{hkl\}}$ is varied in the range $\gamma^{s\prime}_{\{hkl\}}/2$ and $3\gamma^{s\prime}_{\{hkl\}}/2$, where $\gamma^{s\prime}_{\{hkl\}}$ may be obtained from ab initio computations of the surface free energies in vacuum. For the current analysis, $\gamma^{s\prime}_{\{hkl\}}$ for {111} and {100} crystal facets are obtained from the calculations in Galanakis et al.[36] and are tabulated in the Supporting Information.

Now that the significant energy contributions—the elastic strain energy of the disclination line defects (W_V), the unstrained surface energies ($\gamma^s_{\{hkl\}}$), and the surface stress factor (g)—are accounted for, the transition radii and the stability regimes for MTPs are computed using eq 1. [In Table S2 of the Supporting Information, the transition radii computed for g = 0.5 are tabulated and compared to the size ranges obtained using atomistic simulations for silver and gold,[16] which are observed to be similar in magnitude.] Using the surface stress approximations described above and eliminating the common free energy of formation term ($\Delta\bar{G}_f$), the free energy for any morphology can be written as

$$G = V(W_V) + (A_{\{111\}}\gamma^s_{\{111\}} + A_{\{100\}}\gamma^s_{\{100\}})(1 + g\bar{e}_s) + \gamma^s_t A_t \quad (4)$$

The parameters $\gamma^s_{\{111\}}$, $\gamma^s_{\{100\}}$, and g are influenced by changing the environmental conditions. To illustrate the effect of g on the transition radii, we show the variations in $r_{Ic\to Sc}$ and $r_{Dh\to Sc}$ by plotting $G/V^{2/3}$ as a function of equivalent radius r_{eq} (defined as the radius of a sphere of volume V, $r_{eq} = (3V/4\pi)^{1/3}$) in Figure 2. The parameters used are $\gamma^s_{\{111\}} = 1.128$ J/m^2 and $\gamma^s_{\{100\}} = 1.245$ J/m^2 for silver.[36] We choose two values of g such that for g = 0.50 the usual trend of Ic → Dh → Sc is observed, and for g = 0.80 a direct transition from Ic→Sc is obtained.

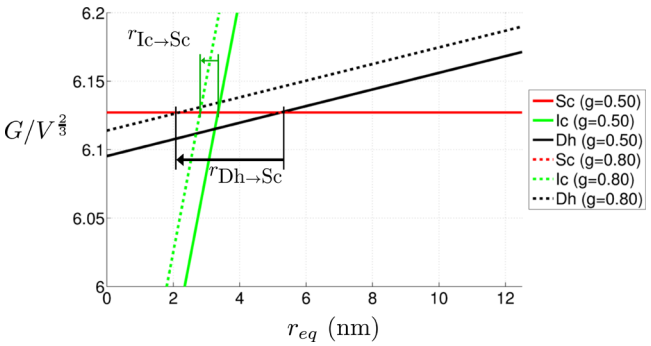

Figure 2. Free energies of silver nanoparticles with Ic (green), Dh (black) and Sc (red) morphologies for surface stress factors g = 0.50 (solid) and g = 0.80 (dotted). The changes in the transition radii $r_{Dh\to Sc}$ and $r_{Ic\to Sc}$ are illustrated. The two values of g are picked such that for g = 0.50 the usual trend of Ic → Dh → Sc is observed, and for g = 0.80, the Dh morphology is thermodynamically unstable.

These plots contain straight lines with slopes proportional to the elastic strain energy of the disclination defect W_V. W_V^{Dh} is approximately 1 order of magnitude smaller than W_V^{Ic} (refer to Table 1). The slope of the line corresponding to the single crystal Wulff shape is zero since $W_V^{Sc} = 0$. The intercepts of these lines, which are proportional to the surface energy contribution, change as g is modified. Increasing g decreases the transition radii $r_{Dh\to Sc}$ and $r_{Ic\to Sc}$. However, since the slope of the line corresponding to the Dh morphology is significantly lower than that corresponding to the Ic morphology, the change in the transition radius $r_{Dh\to Sc}$ is much higher than the change in $r_{Ic\to Sc}$. Therefore, the surface stress factor g may be increased to inhibit the formation of Dh particles, as shown in Figure 2.

dx.doi.org/10.1021/jz401496d | J. Phys. Chem. Lett. 2013, 4, 3089−3094

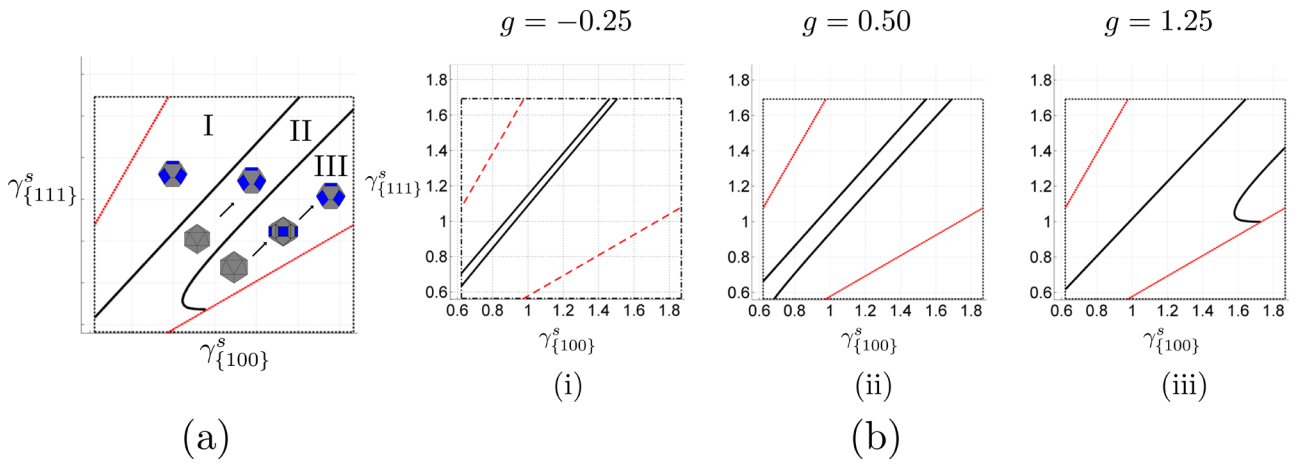

Figure 3. (a) A typical stability map for icosahedral and decahedral nanoparticles with varying unstrained surface energies ($\gamma^s_{\{111\}}$ and $\gamma^s_{\{100\}}$) is shown. Since we consider the strong-faceting model, only the regions between the red dashed lines corresponding to $1/\sqrt{3} \le \gamma^s_{\{111\}}/\gamma^s_{\{100\}} \le \sqrt{3}$ are relevant. There exist three regions: (i) In Region I, the MTPs are thermodynamically never stable, (ii) the Dh morphologies are thermodynamically unstable in Region II, and we observe a direct transition from Ic to Sc, and (iii) in Region III, we obtain the conventional trend of the Ic→Dh→Sc transition. (b) The sizes of the three regions vary as the surface stress factor g is changed, and this is illustrated by computing the stability regimes for Ic, Dh, and Sc morphologies for (i) $g = -0.25$, (ii) $g = 0.50$, and (iii) $g = 1.25$. Increasing g results in an increase in the size of Region II, increasing the likelihood of the formation of metastable Ic structures.

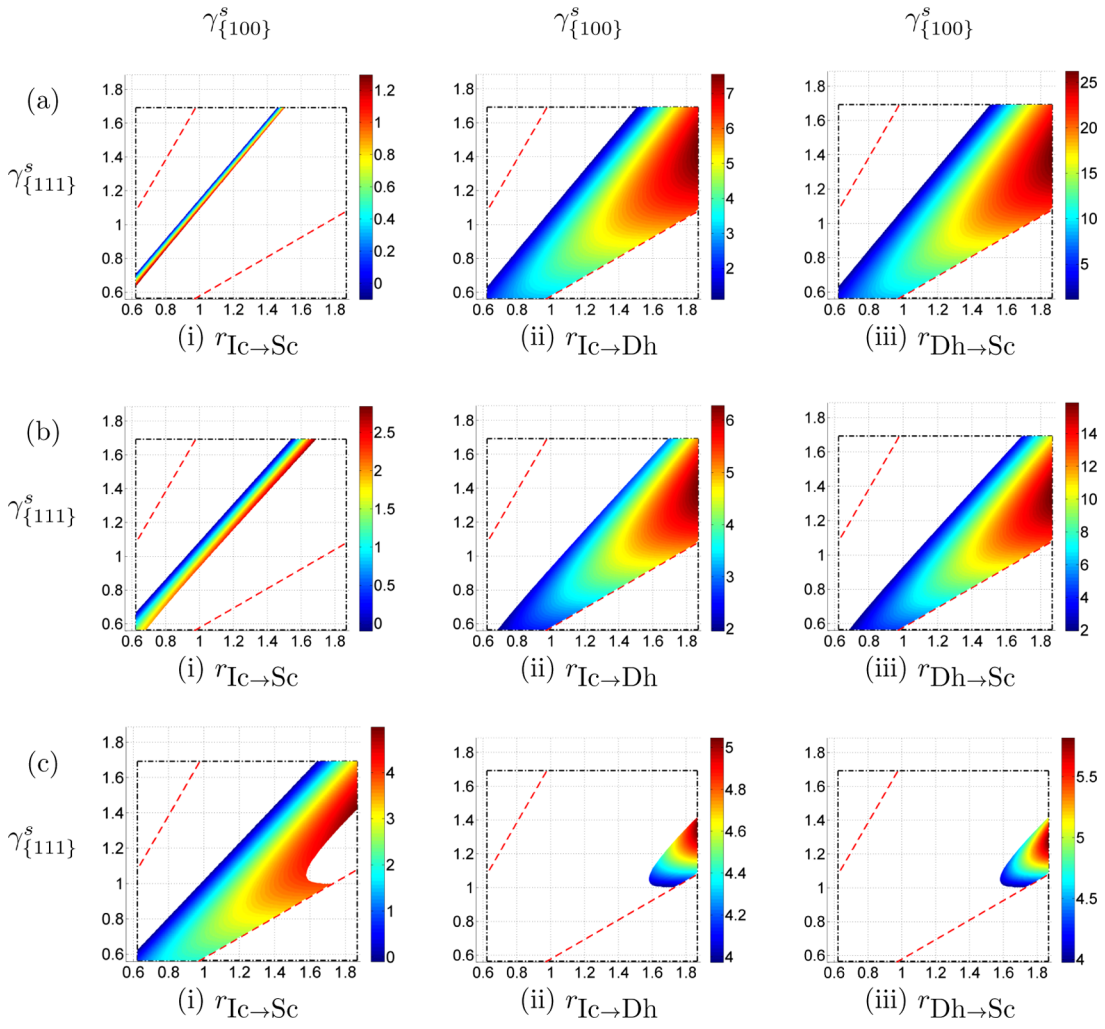

Figure 4. Plots of the transition radii (i) $r_{Ic\to Sc}$ in region II, (ii) $r_{Ic\to Dh}$ in region III and (iii) $r_{Dh\to Sc}$ in region III, for (a) $g = -0.25$, (b) $g = 0.50$ and (c) $g = 1.25$ for silver with $\gamma^s_{\{hkl\}}$ in the interval $[\gamma^{s\prime}_{\{hkl\}}/2, 3\gamma^{s\prime}_{\{hkl\}}/2]$.

dx.doi.org/10.1021/jz401496d | J. Phys. Chem. Lett. 2013, 4, 3089−3094

Variations in the surface stress factor g can be accomplished through many means; for example, by tailoring the solution chemistry in which the nanoparticles are grown. Changing the solution chemistry in turn modifies the surface energies. Even though surface energies ($\gamma^s_{\{hkl\}}$) and the surface stress factor (g) refer to different physical quantities, it may be difficult to control these parameters individually. Therefore, the analysis of the stability regimes while simultaneously varying $\gamma^s_{\{hkl\}}$ and g is necessary. When g is held constant, a phase map such as the one shown in Figure 3a is typical, which consists of three distinct regions. In the first region (Region I), the MTPs are never thermodynamically stable and the nanoparticle nucleation occurs directly as single crystal Wulff shapes. In the second region (Region II), the Dh morphology is unstable and the direct transition from the icosahedra to the single crystal Wulff shapes occurs under thermodynamic growth conditions. The third region (Region III) is where the conventional trend of transitions from the icosahedra to the decahedra to the single crystal Wulff shapes occur as the particle grows. The effect of varying the surface stress factor on the sizes of these three regimes is shown in Figure 3b. Increasing g increases the size of Region II, resulting in thermodynamic growth conditions where the transition from the Ic to the Dh morphologies may be avoided.

To understand the influence of tailoring solution chemistry on the transition radii, we plot the transition radii $r_{Ic\rightarrow Sc}$, $r_{Ic\rightarrow Dh}$ and $r_{Dh\rightarrow Sc}$ in Figure 4 for silver (and in Figure S2 in the Supporting Information for gold). It is possible to create thermodynamic growth conditions that inhibit the formation of the Dh structures and increase the transition radius from the Ic to the Sc morphologies. For example, as shown in the legends in Figures 4(i) and S2(i), the maximum possible $r_{Ic\rightarrow Sc}$ increases with increasing g. Similarly, it is possible to stabilize large ($\approx$ 25 nm) Dh morphologies by decreasing g and appropriately modifying $\gamma^s_{\{hkl\}}$ (Figures 4a(iii) and S2a(iii)).

At the nanoscale, icosahedral and decahedral structures offer improved performance and new prospects for a variety of metallic nanoparticle technologies. Therefore, it is essential to precisely control the synthesis of these multiply twinned nanoparticles. However, the thermodynamic and kinetic underpinnings of the growth of nanoparticles are not well established. In this Letter, we present a mesoscale thermodynamic analysis with varying surface free energy and surface stress parameters to account for a variety of growth conditions. To facilitate rigorous thermodynamic analysis of the Ic and Dh structures, we compute the elastic strain energies of the disclination line defects using finite element analysis in ABAQUS.

To investigate the influence of varying the solution chemistry on the stability of the Ic and Dh nanoparticles, the parameters that are sensitive to environmental conditions are isolated and varied. These parameters include the free energy of an unstrained surface (γ^s) and the variation in the surface free energy due to applied strain, which is quantified by the surface stress factor g. γ^s has been established as an important parameter for controlling the morphology and the transition radii among various structures. We show that the surface stress factor g also plays an important role in controlling the stability of MTPs. Modifying the surface free energies γ^s and increasing the surface stress factor g increases the likelihood of obtaining large metastable Ic morphologies. Similarly, large Dh shaped nanoparticles may be obtained by decreasing g. Therefore, the surface stress factor g should be considered as an important design parameter in the synthesis of multiply twinned nanoparticles.

Prior experimental reports are primarily concerned with adsorbate-induced variations of surface stresses.[37] For example, adsorption of hydrogen or oxygen on the Pt {111} surface relieves the tensile surface stress resulting in a decrease in the surface stress factor g. This relaxation depends on the loading (concentration of hydrogen or oxygen) in the environment and the extent of relaxation due to oxygen adsorption is approximately 3 times the relaxation induced by hydrogen.[38] Surface stress relaxation due to oxygen adsorption has been utilized to chemically induce actuation in nanoporous gold.[39] In the case of CO adsorption on the Ni{100} surface, an initial increase in the surface stress is detected, however, stress relaxation is observed on further loading.[40] Carbon adsorption on the Ni{111} surface also results in surface stress relaxation and the effect is strong enough that the final surface stress state is compressive, which implies a negative g value.[40] Surfactants might have a similar effect on the surface stress during the growth of nanoparticles in solutions.

Surface stresses may also be manipulated during the solution synthesis by introducing other metal ions, which could either form a monolayer or a bimetallic film on the surface of the growing nanoparticle. For example, the presence of silver monolayer on Pt{100} and {111} surfaces reduces the tensile surface stress.[41] A bimetallic film on the surface of a nanoparticle could also reduce g through segregation and pattern formation.[42]

Experimental investigations of adsorbate-induced changes in surface stresses clearly indicate that g can be tailored, and, depending on the solution chemistry, g can either be negative or positive. Unfortunately, the origins of stress-relief (or enhancement) mechanisms are not completely understood (a discussion on the different mechanisms and their drawbacks is provided by Sander[37]). Further experimental and theoretical analyses discerning these mechanisms are necessary for developing a rational solvent selection process in nanoparticle synthesis.

■ ASSOCIATED CONTENT

Supporting Information

Details of the finite element analysis of the icosahedron model, material parameters, stability map for gold and an estimate for the surface stress factor g are included. This material is available free of charge via the Internet at http://pubs.acs.org/.

■ AUTHOR INFORMATION

Corresponding Author

*E-mail: m-olvera@northwestern.edu.

Present Address

$^{\perp}$(S.P.) Department of Materials Science and Engineering, North Carolina State University, Raleigh, North Carolina 27606, United States.

Notes

The authors declare no competing financial interest.

■ ACKNOWLEDGMENTS

This work is supported by the NSF MRSEC program grant number DMR-1121262 and the Northwestern Materials Research Science and Engineering Center. We also thank Dr. Emilie Ringe for critical reading of the manuscript.

REFERENCES

(1) Ino, S. Epitaxial Growth of Metals on Rocksalt Faces Cleaved in Vacuum. II. Orientation and Structure of Gold Particles Formed in Ultrahigh Vacuum. *J. Phys. Soc. Jpn.* **1966**, *21*, 346−362.

(2) Ino, S. Stability of Multiply-Twinned Particles. *J. Phys. Soc. Jpn.* **1969**, *27*, 941−953.

(3) Kuai, L.; Geng, B.; Wang, S.; Zhao, Y.; Luo, Y.; Jiang, H. Silver and Gold Icosahedra: One-Pot Water-Based Synthesis and Their Superior Performance in the Electrocatalysis for Oxygen Reduction Reactions in Alkaline Media. *Chem.—Eur. J.* **2011**, *17*, 3482−3489.

(4) Wu, J.; Qi, L.; You, H.; Gross, A.; Li, J.; Yang, H. Icosahedral Platinum Alloy Nanocrystals with Enhanced Electrocatalytic Activities. *J. Am. Chem. Soc.* **2012**, *134*, 11880−11883.

(5) Karna, S.; Li, C.; Wu, C.; Hsu, C.; Wang, C.; Li, W. Observations of Large Magnetic Moments in Icosahedral Pb Nanoparticles. *J. Phys. Chem. C* **2011**, *115*, 8906−8910.

(6) Wang, R.; Dmitrieva, O.; Farle, M.; Dumpich, G.; Ye, H.; Poppa, H.; Kilaas, R.; Kisielowski, C. Layer Resolved Structural Relaxation at the Surface of Magnetic FePt Icosahedral Nanoparticles. *Phys. Rev. Lett.* **2008**, *100*, 17205.

(7) Wang, R.; Dmitrieva, O.; Farle, M.; Dumpich, G.; Acet, M.; Mejia-Rosales, S.; Perez-Tijerina, E.; Yacaman, M.; Kisielowski, C. FePt Icosahedra with Magnetic Cores and Catalytic Shells. *J. Phys. Chem. C* **2009**, *113*, 4395−4400.

(8) Qiu, J.; Wang, J. Tuning the Crystal Structure and Magnetic Properties of FePt Nanomagnets. *Adv. Mater.* **2007**, *19*, 1703−1706.

(9) Liu, M.; Guyot-Sionnest, P. Mechanism of Silver(I)-Assisted Growth of Gold Nanorods and Bipyramids. *J. Phys. Chem. B* **2005**, *109*, 22192−22200.

(10) Pietrobon, B.; McEachran, M.; Kitaev, V. Synthesis of Size-Controlled Faceted Pentagonal Silver Nanorods with Tunable Plasmonic Properties and Self-Assembly of These Nanorods. *ACS Nano* **2009**, *3*, 21−26.

(11) Sánchez-Iglesias, A.; Pastoriza-Santos, I.; Pérez-Juste, J.; Rodríguez-González, B.; García de Abajo, F. J.; Liz-Marzán, L. M. Synthesis and Optical Properties of Gold Nanodecahedra with Size Control. *Adv. Mater.* **2006**, *18*, 2529−2534.

(12) Pastoriza Santos, I.; Sánchez Iglesias, A.; Garcia de Abajo, F.; Liz-Marzan, L. Environmental optical sensitivity of gold nano-decahedra. *Adv. Funct. Mater.* **2007**, *17*, 1443−1450.

(13) Pietrobon, B.; Kitaev, V. Photochemical Synthesis of Monodisperse Size-Controlled Silver Decahedral Nanoparticles and Their Remarkable Optical Properties. *Chem. Mater.* **2008**, *20*, 5186−5190.

(14) Walsh, M.; Yoshida, K.; Kuwabara, A.; Pay, M.; Gai, P.; Boyes, E. On the Structural Origin of the Catalytic Properties of Inherently Strained Ultrasmall Decahedral Gold Nanoparticles. *Nano Lett.* **2012**, *12*, 2027−2031.

(15) Cleveland, C. L.; Landman, U. The Energetics and Structure of Nickel Clusters: Size Dependence. *J. Chem. Phys.* **1991**, *94*, 7376−7396.

(16) Baletto, F.; Ferrando, R.; Fortunelli, A.; Montalenti, F.; Mottet, C. Crossover among Structural Motifs in Transition and Noble-Metal Clusters. *J. Chem. Phys.* **2002**, *116*, 3856−3863.

(17) Baletto, F.; Ferrando, R. Structural Properties of Nanoclusters: Energetic, Thermodynamic, and Kinetic Effects. *Rev. Mod. Phys.* **2005**, *77*, 371−423.

(18) Kuo, C.-L.; Clancy, P. Melting and Freezing Characteristics and Structural Properties of Supported and Unsupported Gold Nanoclusters. *J. Phys. Chem. B* **2005**, *109*, 13743−13754.

(19) Angulo, A. M.; Noguez, C. Atomic Structure of Small and Intermediate-Size Silver Nanoclusters. *J. Phys. Chem. A* **2008**, *112*, 5834−5838.

(20) Xiong, Y.; McLellan, J. M.; Yin, Y.; Xia, Y. Synthesis of Palladium Icosahedra with Twinned Structure by Blocking Oxidative Etching with Citric Acid or Citrate Ions. *Angew. Chem.* **2007**, *119*, 804−808.

(21) Seo, D.; Yoo, C. I.; Im Sik, C.; Park, S. M.; Ryu, S.; Song, H. Shape Adjustment between Multiply Twinned and Single-Crystalline Polyhedral Gold Nanocrystals: Decahedra, Icosahedra, and Truncated Tetrahedra. *J. Phys. Chem. C* **2008**, *112*, 2469−2475.

(22) Xia, Y.; Xiong, Y.; Lim, B.; Skrabalak, S. E. Shape-Controlled Synthesis of Metal Nanocrystals: Simple Chemistry Meets Complex Physics? *Angew. Chem., Int. Ed.* **2008**, *48*, 60−103.

(23) Zhang, Q.; Xie, J.; Yang, J.; Lee, J. Y. Monodisperse Icosahedral Ag, Au, and Pd Nanoparticles: Size Control Strategy and Superlattice Formation. *ACS nano* **2009**, *3*, 139−148.

(24) Lim, B.; Jiang, M.; Tao, J.; Camargo, P. H.; Zhu, Y.; Xia, Y. Shape-Controlled Synthesis of Pd Nanocrystals in Aqueous Solutions. *Adv. Funct. Mater.* **2009**, *19*, 189−200.

(25) Langille, M.; Zhang, J.; Mirkin, C. Plasmon-Mediated Synthesis of Heterometallic Nanorods and Icosahedra. *Angew. Chem., Int. Ed.* **2011**, *50*, 3543−3547.

(26) Gonzalez, A. L.; Noguez, C.; Barnard, A. Map of the Structural and Optical Properties of Gold Nanoparticles at Thermal Equilibrium. *J. Phys. Chem. C* **2012**, *116*, 14170−14175.

(27) Patala, S.; Marks, L.; Olvera de la Cruz, M. Elastic Strain Energy Effects in Faceted Decahedral Nanoparticles. *J. Phys. Chem. C* **2013**, *117*, 1485−1494.

(28) Marks, L. Surface Structure and Energetics of Multiply Twinned Particles. *Philos. Mag. A* **1984**, *49*, 81−93.

(29) Howie, A.; Marks, L. Elastic Strains and the Energy Balance for Multiply Twinned Particles. *Philos. Mag. A* **1984**, *49*, 95−109.

(30) DeWit, R. Partial Disclinations. *J. Phys. C: Solid State Phys.* **1972**, *5*, 529−534.

(31) Johnson, C. L.; Snoeck, E.; Ezcurdia, M.; Rodríguez-González, B.; Pastoriza-Santos, I.; Liz-Marzán, L. M.; Hÿtch, M. J. Effects of Elastic Anisotropy on Strain Distributions in Decahedral Gold Nanoparticles. *Nat. Mater.* **2007**, *7*, 120−124.

(32) ABAQUS, *ABAQUS/Standard Version 6.11−1*; Dassault Systémes Simulia Corp.: Providence, RI, 2011.

(33) Bower, A. Constitutive Models: Relations between Stress and Strain. In *Applied Mechanics of Solids*; CRC Press: Boca Raton, FL, 2009; pp 91−93.

(34) Cahn, J. W. Surface Stress and the Chemical Equilibrium of Small Crystals−I. The Case of the Isotropic Surface. *Acta Metall.* **1980**, *28*, 1333−1338.

(35) Cammarata, R.; Sieradzki, K. Surface and Interface Stresses. *Annu. Rev. Mater. Sci.* **1994**, *24*, 215−234.

(36) Galanakis, I.; Bihlmayer, G.; Bellini, V.; Papanikolaou, N.; Zeller, R.; Blügel, S.; Dederichs, P. Broken-Bond Rule for the Surface Energies of Noble Metals. *Europhys. Lett.* **2002**, *58*, 751.

(37) Sander, D. Surface Stress: Implications and Measurements. *Curr. Opin. Solid State Mater. Sci.* **2003**, *7*, 51−57.

(38) Feibelman, P. J. First-Principles Calculations of Stress Induced by Gas Adsorption on Pt(111). *Phys. Rev., B: Condens. Matter* **1997**, *56*, 2175−2182.

(39) Biener, J.; Wittstock, A.; Zepeda-Ruiz, L.; Biener, M.; Zielasek, V.; Kramer, D.; Viswanath, R.; Weissmüller, J.; Bäumer, M.; Hamza, A. Surface-Chemistry-Driven Actuation in Nanoporous Gold. *Nat. Mater.* **2008**, *8*, 47−51.

(40) Ibach, H. The Role of Surface Stress in Reconstruction, Epitaxial Growth and Stabilization of Mesoscopic Structures. *Surf. Sci. Rep.* **1997**, *29*, 195−263.

(41) Batzill, M.; Koel, B. Silver on Pt (100): Alloying vs. Surface Reconstruction−Two Competing Mechanisms to Reduce Surface Stress. *Europhys. Lett.* **2003**, *64*, 70−76.

(42) Thayer, G.; Ozolins, V.; Schmid, A.; Bartelt, N.; Asta, M.; Hoyt, J.; Chiang, S.; Hwang, R. Role of Stress in Thin Film Alloy Thermodynamics: Competition between Alloying and Dislocation Formation. *Phys. Rev. Lett.* **2001**, *86*, 660−663.